Physics of Plasmas

Terahertz radiation enhanced by target ablation during the interaction of high intensity laser pulse and micron-thickness metal foil

Cite as: Phys. Plasmas **27**, 023101 (2020); https://doi.org/10.1063/1.5125611
Submitted: 24 August 2019 . Accepted: 11 December 2019 . Published Online: 03 February 2020

Siyuan Zhang, Jinqing Yu, Yinren Shou, Zheng Gong, Dongyu Li, Yixing Geng, Weimin Wang, Xueqing Yan, and Chen Lin

Physics of Plasmas ARTICLE scitation.org/journal/php

Terahertz radiation enhanced by target ablation during the interaction of high intensity laser pulse and micron-thickness metal foil

Cite as: Phys. Plasmas **27**, 023101 (2020); doi: 10.1063/1.5125611
Submitted: 24 August 2019 · Accepted: 11 December 2019 ·
Published Online: 3 February 2020

Siyuan Zhang,[1] Jinqing Yu,[2] Yinren Shou,[1] Zheng Gong,[1] Dongyu Li,[1] Yixing Geng,[1] Weimin Wang,[3] Xueqing Yan,[1,4] and Chen Lin[1,4,a)]

AFFILIATIONS

[1]State Key Laboratory of Nuclear Physics and Technology, and Key Laboratory of HEDP of the Ministry of Education, CAPT, Peking University, Beijing 100871, China
[2]School of Physics and Electronics, Hunan University, Changsha, 410082, China
[3]Department of Physics and Beijing Key Laboratory of Opto-electronic Functional Materials and Micro-nano Devices, Renmin University of China, Beijing 100872, China
[4]Collaborative Innovation Center of Extreme Optics, Shanxi University, Shanxi, China, 030006

[a)]Electronic mail: lc0812@pku.edu.cn

ABSTRACT

When an ultra-intense relativistic laser is irradiated on a solid target, terahertz (THz) pulses can be generated by coherent transition radiation when the laser-driven electron beams cross the rear surface of the target. The radiation energy depends on the number and energy of the electrons. By introducing a milli-joule picosecond ablation laser pulse, an underdense preplasma with a scale length of micrometers is generated at the front surface of the target. Electron beams with more charge and higher energy can be produced during the interaction between the following main laser pulse and the preplasma, which enhance the THz radiation and affect the radiation angle. Two dimensional particle-in-cell simulations demonstrate the improvement of electron beams and a nearly tenfold enhancement of THz radiation energy is observed.

I. INTRODUCTION

High power terahertz (THz) sources are important tools in many research fields[1,2] including materials science,[3] biomedical imaging,[4] wireless communication,[5] and astronomy.[6] THz radiation can be generated by various approaches, such as photoconductive antenna,[7–9] optical rectification,[10,11] and dual-color-laser-excited air plasma.[12] THz yield from these approaches increases with the pump laser intensity and saturates at the laser intensity around 10^{15} W/cm^2.

Instead of being limited by the saturation of THz sources driven by pump laser pulses with a nonrelativistic intensity, THz yield from relativistic electron does not show any tendency of saturation. Based on the transition radiation,[13] synchrotron radiation,[14] diffraction radiation,[15] and Cherenkov radiation[16] of relativistic electron beams, strong THz radiation has been realized theoretically and experimentally. Among the several methods mentioned above, transition radiation has the advantage of achieving THz source with high energy. Recently, the experiment has reported that the energy of THz radiation from relativistic electron beams by transition radiation based on conventional linear accelerator has reached 600 μJ/pulse.[17] However, the size scale of the conventional large accelerator definitely limits the relevant applications of these kinds of THz sources, which appeals to an alternative more feasible way to generate the THz radiation.

With the rapid progress of the state-of-the-art laser technology,[18,19] the laser intensity has already been beyond the criterion of relativistic intensity, i.e., 10^{18} W/cm^2. Based on the interaction between relativistically intense laser pulses and plasmas, the generated compact THz resources will significantly reduce the volume and cost of the facilities. This ultrashort THz radiation is predominantly emitted by the energetic electron beams which are produced from laser–gas and laser–solid interactions.[20–23] In laser–gas interactions, electrons can be accelerated to GeV magnitude,[24] and THz pulses with energy of $\sim$0.3 μJ have been generated.[25] In laser–solid interactions, THz radiation can be generated by various mechanisms: At the front side of the target, THz radiation is attributed to the mode conversion and the transient current at the plasma–vacuum interface. As the scale length of preplasma changes, the dominant laser–plasma

interaction is different (e.g., from resonance absorption to parametric instabilities) and the terahertz radiation yield varies,[26,27] while at the rear side of the target, terahertz radiation is produced through coherent transition radiation (CTR) when hot electrons cross the target–vacuum surface.[28] Due to the high density of solid, electron beams with charge up to μC–nC can be generated and THz radiations with energies up to 50 mJ have been reported.[29–32]

It should be noticed that the energy conversion efficiency from pump laser pulse to THz radiation in laser–solid interactions is small, for example, in the magnitude of 0.01% (Ref. 32) from femtosecond laser interacting with a foil target. The theory of CTR[33] indicates that the radiation energy is proportional to $N(N-1)$, where N is the number of electrons in the generated ultrashort electron pulse. Therefore, a key method to enhance THz yield is to increase the charge of electron beams to improve the coherence effect, which means one can either use laser pulses with higher intensity[21] or increase the energy deposition rate.

In order to raise the energy deposition from the laser pulse to electron beams, we propose to utilize the preplasma generated by the laser target ablation to improve the laser-plasma coupling efficiency.[34–37] As far as we know, the effect of large preplasma scale length (larger than 5 μm) on terahertz radiation behind the target has never been studied. It is worth pointing out that the effects of laser contrast ratio and large scale preplasma on terahertz radiation in front of the target have been experimentally investigated.[26,27] Here, our schematic of setup is shown in Fig. 1. First, the ablation pulse induces ablation on the front surface of an aluminum target and the preplasma with micrometers density scale length is produced; then the relativistic main laser pulse is irradiated on the target perpendicularly. The scale length of preplasma can be varied through the time delay between the ablation pulse and the main pulse.

In addition, the plasma electron density of preplasma induced by the ablation tends to be underdense or near critical.[38] When the main pulse propagates in the preplasma, it will experience relativistic

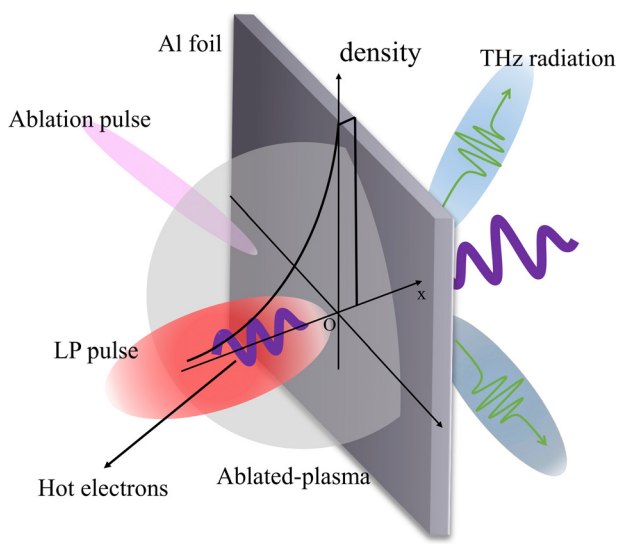

FIG. 1. The schematic of the setup. A linearly polarized laser pulse (red) generates energetic electrons when it propagates in the preplasma (gray) caused by the ablation laser pulse (pink). When these fast electrons cross the rear target surface, THz pulses are produced via the transition radiation.

self-focusing,[39,40] which can increase the laser intensity and boost the electron heating process through various mechanisms such as resonance absorption,[41] $J\times B$ heating,[42] and ponderomotive acceleration.[43] With the increase in the preplasma scale length, stochastic heating[44] and various parametric instabilities can take place[45,46] as well. Under the proper matching condition of plasma's density and scale length, the main laser pulse is able to drive a plasma channel with a strong quasi-static azimuthal magnetic field. Electrons captured in the plasma channel will undergo direct laser acceleration (DLA),[47–52] generating collimated electrons with higher energy density. All these mechanisms facilitate the generation of hot dense electrons which lead to the stronger transition radiation compared to the condition without ablation when electrons cross the rear surface of the target.

In this work, we study the energy and angular-spectral distribution of the THz pulse generated through interactions between laser pulses and metal foils in the conditions with and without laser ablation. Particle-in-cell (PIC) simulations show that electron beam with more charge and higher energy can be produced by the driven laser pulse when the target ablation takes place. Through the numerical calculation of THz radiation energy, a nearly tenfold enhancement is observed in a large angular range.

II. COHERENT TRANSITION RADIATION BY ELECTRON BEAMS

When electrons cross the plasma–vacuum boundary, a lateral polarization current will be generated at the interface due to the dielectric discontinuity, thereby emitting transition radiation.[53] In the incidence plane, the energy spectrum of the transition radiation from a single electron passing through a target surface can be written as[33]

$$\frac{d^2\mathscr{E}}{d\omega d\Omega}=\frac{e^2}{\pi^2 c}|S(\beta,\varphi,\phi)|^2, \tag{1}$$

where e is the electron charge, c is the light velocity in vacuum, β is the normalized velocity, φ is the electron injection direction, ϕ is the observation direction, and

$$S(\beta,\varphi,\phi)=\frac{\beta\cos\varphi(\sin\phi-\beta\sin\varphi)}{(1-\beta\sin\phi\sin\varphi)^2-(\beta\cos\phi\cos\varphi)^2}. \tag{2}$$

Angular distribution of transition radiation is plotted in Fig. 2, where the electron is perpendicularly injected into the dense plasma–vacuum interface. There are two symmetric peaks on either side of the incidence direction. It can be seen that when the electron has low energy such as 0.1 MeV, the radiation is strongest along the target surface. When the electron carries larger kinetic energy, e.g., 10 MeV, the radiation becomes more collimated and close to the electron injection direction.

For a pulsed beam with N electrons inside the bunch and a density distribution function of $g(\boldsymbol{p})$, where $\boldsymbol{p}$ is the momentum of electron, the radiation emitted per unit solid angle per unit angular frequency by the particle beam crossing the boundary is given by[54]

$$\frac{d^2W}{d\omega d\Omega}=\frac{e^2N}{\pi^2 c}\int d^3\boldsymbol{p}\left(\varepsilon_{\parallel}^2+\varepsilon_{\perp}^2\right)g(\boldsymbol{p})+\frac{e^2N(N-1)}{\pi^2 c}\left(\left|\int d^3\boldsymbol{p}g(\boldsymbol{p})\varepsilon_{\parallel}F\right|^2+\left|\int d^3\boldsymbol{p}g(\boldsymbol{p})\varepsilon_{\perp}F\right|^2\right), \tag{3}$$

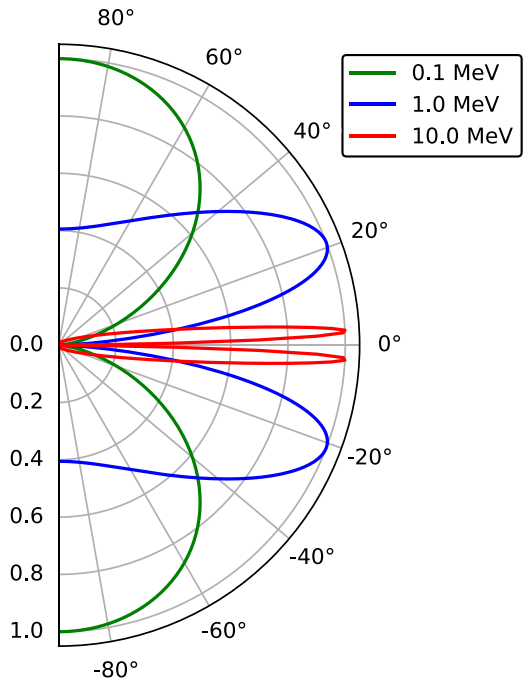

FIG. 2. Angular distributions of the transition radiation generated by a single electron with different energies of 0.1 MeV (green), 1.0 MeV (blue), and 10.0 MeV (red). Each distribution is normalized by its own maximum.

where $\varepsilon_{||}$ and $\varepsilon_{\perp}$ are the Fourier transforms of electric field in the parallel and perpendicular radiation planes. F is the spatial form factor of electron beams which is correlated with the geometry of the beam.[54] On the right-hand side of the equation, the first term is incoherent transition radiation (ITR) and the second term is CTR.

The electron beams generated during laser–solid interactions are usually considered to have a waist of a few micrometers and a duration of femtoseconds to picoseconds, which are consistent with spot size and pulse duration of the driven laser. Both the radius and duration are shorter than the wavelength of 30 THz (10 μm). In addition, the incoherent transition radiation ($\propto N$) is many orders of magnitudes weaker than the coherent transition radiation [$\propto N(N-1)$]. As a result, the dominant THz generation mechanism at the rear surface of the target is considered to be CTR for 0.1–30 THz.

III. SIMULATION RESULTS

In our study, an ablation laser pulse of table envelope with 200 ps duration and 25 mJ energy is irradiated on the front surface of an aluminum foil target with a 2.5 μm thickness and 2.7 g/cm^3 density. The laser intensity is 2.1×10^{12} W/cm^2. The ablated preplasma is calculated by the hydrodynamic code MULTI.[55] Figure 3 shows simulation results of the preplasma after different ablation times: (a) density, (b) electron temperature, (c) ionization degree, and (d) the collision frequency. We can see that the expanded near critical density preplasma with a scale of tens of micrometers is generated in the target front surface in the condition with ablation, while the rear surface still keeps a relatively sharp density interface. The collision frequency is calculated by the equation[56] $\nu_{ei} \approx 2.91 \times 10^{-6} Z n_e T_e^{-3/2} \ln\Lambda (s^{-1})$, where Z, n_e, and T_e represent the ionization degree, electron density, and electron temperature, respectively. Here, $\ln\Lambda$ is estimated to be 5.0 according to the temperature and density of electron by the equation $\ln\Lambda = 22.36 + \frac{3}{2}\ln T(\mathrm{eV}) - \frac{1}{2}\ln n(\mathrm{cm}^{-3})$. Figure 3(d) shows that collision frequency is low in the preplasma and the collision can be neglected. With an ultra-intense femtosecond main laser pulse, the electron is heated to MeV energy magnitude and ν_{ei} decreases to about 10^{13} s^{-1} even at the target (around 0 μm), indicating that the collision can be neglected in the following PIC simulation on femtosecond time scale.

Then, the pre-ablated plasma distribution of 200 ps ablation shown in Fig. 3(a) is introduced into the following 2D PIC code EPOCH[57] as the initial plasma condition. Preplasma is set in front of the solid target in both without ablation and with ablation cases. The former is caused by the non-perfect contrast of the main laser (existing of the replica, the Amplified Spontaneous Emission (ASE) and the pedestal), and the latter is caused by the ablation laser pulse. The density profiles of plasma are set as follows: In the condition without ablation, the preplasma has an exponential profile with a scale length of 0.63 μm from 0.1 n_c to 20.0 n_c in consideration of prepulse in the condition of a laser contrast 10^{-10} at 40 ps before the main pulse and a table profile with maximum of 20.0 n_c and thickness of 6.70 μm. Here, $n_c = m_e\omega^2\varepsilon_0/e^2$ is the critical density of the plasma. We set plasma with lower maximum density and larger thickness for computing efficiency. In the condition with ablation, the plasma is divided into three parts to fit the result from MULTI: an exponential profile with a scale length of 16.98 μm from 0.1 n_c to 1.0 n_c, an exponential profile with a scale length of 1.70 μm from 1.0 n_c to 20.0 n_c, and a plateau profile with a length of 0.80 μm. It has been demonstrated that when the maximum plasma density is changed from $10n_c$ to $110n_c$; there is no obvious change in the intensity or profile of the THz radiation.[58] The size of the simulation box is 120 μm in both X and Y direction, which is divided into 6000×3600 grids. The ion is set as Al^{10+} with 3 macro-ions and 30 macro-electrons initialized in each cell. The initial temperature of electrons in the preplasma is set at 600 eV in accordance with the MULTI simulations. A p-polarized laser pulse with a central wavelength 0.8 μm, a normalized amplitude $a_0 = eE/m_e\omega_0 c = 5.0$, and Gaussian spatial and sin^2 temporal profile is irradiated onto the plasma target. The duration of the laser pulse is 30 fs and the focal spot radius is 5 μm. The simulation time is 500 fs.

We can see in Fig. 4(a) that the laser is self-focusing in the ablated preplasma, while transferring its energy to the hot electrons at a high conversion efficiency. According to the simulation result, the laser energy is almost all deposited into the electrons at about 225 fs. On the contrast, without the ablation, a major part of the laser is reflected by the steep plasma critical density surface, as indicated in Fig. 4(b). The limited energy conversion efficiency results in a decrease in the number and energy of hot electrons compared with the ablated condition. Figure 4(c) shows the energy spectra of the forward hot electrons ($p_x > 0$, $E > 0.1$ MeV) at the moment of $t = 250$ fs when electrons reach the rear side of the target and start to emit radiation. The cutoff energy is enhanced from 8 MeV to 50 MeV and the number of hot electrons counted by the summation of energy spectrum is increased by 1.5 times in the ablation case. Figure 4(d) is the total energy of forward electrons vs the delay time between the ablation pulse and the main pulse, calculated through the area of electron energy spectrum from 2D PIC simulation. The conversion efficiency of energy from main laser pulse to forward electrons is enhanced greatly by ablation

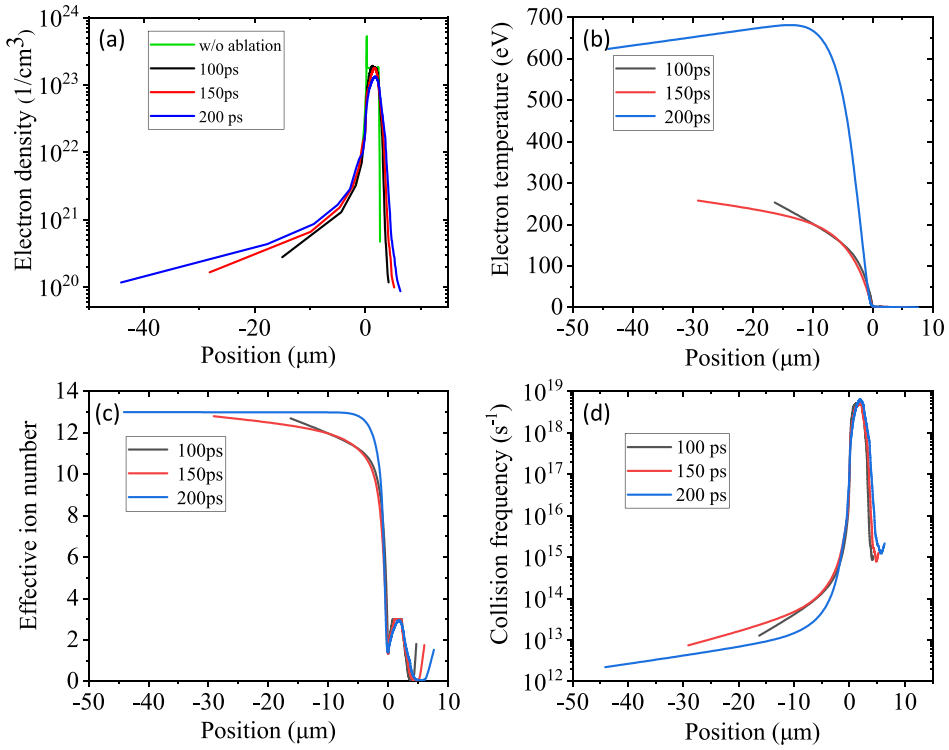

FIG. 3. One dimensional (1d) MULTI Simulation results. (a) Electron density profiles for different time delays between the main pulse and the ablation pulse. (b) and (c) are the profiles for electron temperature and ionization degree simulated by MULTI 1d. (d) Collision frequency between electron and ion calculated from the three distributions above.

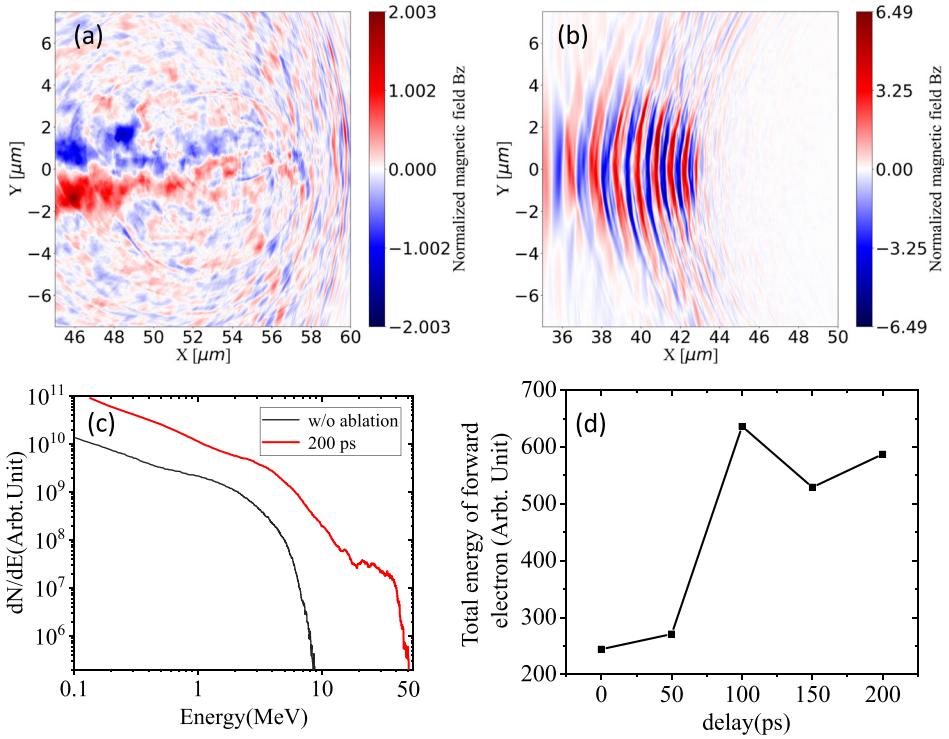

FIG. 4. (a) The spatial distribution of magnetic field Bz at time t = 225 fs in the condition with 200 ps ablation, the laser pulse undergoes self-focusing, and most of its energy is transferred to preplasma. (b)The spatial distribution of magnetic field Bz at time t = 300 fs in the condition without ablation; the majority of the laser pulse is reflected. (c) Energy spectra of forward hot electrons ($P_x > 0$, $E > 0.1$ MeV) in the target at $t = 250$ fs for both conditions. (d) The total energy of forward electrons vs the time delay between the ablation pulse and the main pulse.

and gets to saturation when the time delay is above 100 ps. The reason might be the preplasma is long enough for all laser energy transferring into preplasma electrons.

Figure 5 is the angular-spectral distribution of electrons at t = 250 fs. Ψ represents the direction of electron motion calculated by P_y/P_x, where P_x and P_y are the momentum of electrons in x and y direction, respectively. Compared with the without ablation condition, the electrons show two distinct distributions in the condition of 200 ps ablation. For the electrons with energy less than 10 MeV and large divergence angle, the charge is enhanced significantly, indicating the increase in energy conversion efficiency from laser to electrons. In the meantime, collimated electrons with energy higher than 20 MeV are generated via the mechanism of DLA.[47–52]

Snapshots of the magnetic fields B_z at the simulation time of 400 fs are shown in Fig. 6(a) without ablation and (b) with 200 ps ablation. In the without ablation case, multiple peaks occur in both forward and backward radiation due to the hot electron refluxing processes:[59] When forward electrons cross the rear surface of the target, the first forward THz pulse is produced and most electrons are pulled back by the static electric field near the rear surface. When those electrons cross the front surface of the target, backward radiation is generated, and then the majority of electrons are dragged back by the static electric field near the front surface, generating the second forward THz pulse. While with the present of the ablation preplasma, forward radiation field becomes dominant.

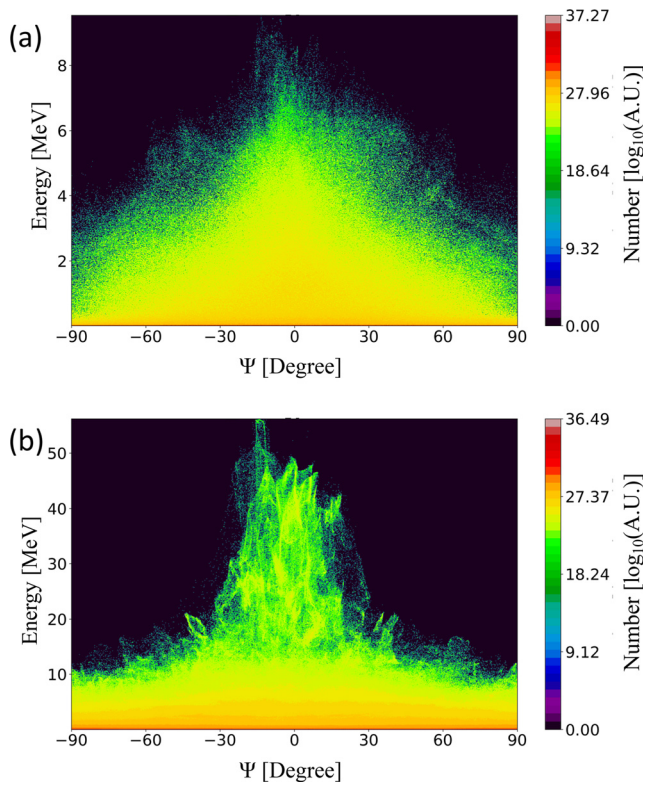

FIG. 5. The angular-spectral distribution of electrons at $t = 250$ fs in the condition without ablation (a) and with 200 ps ablation (b).

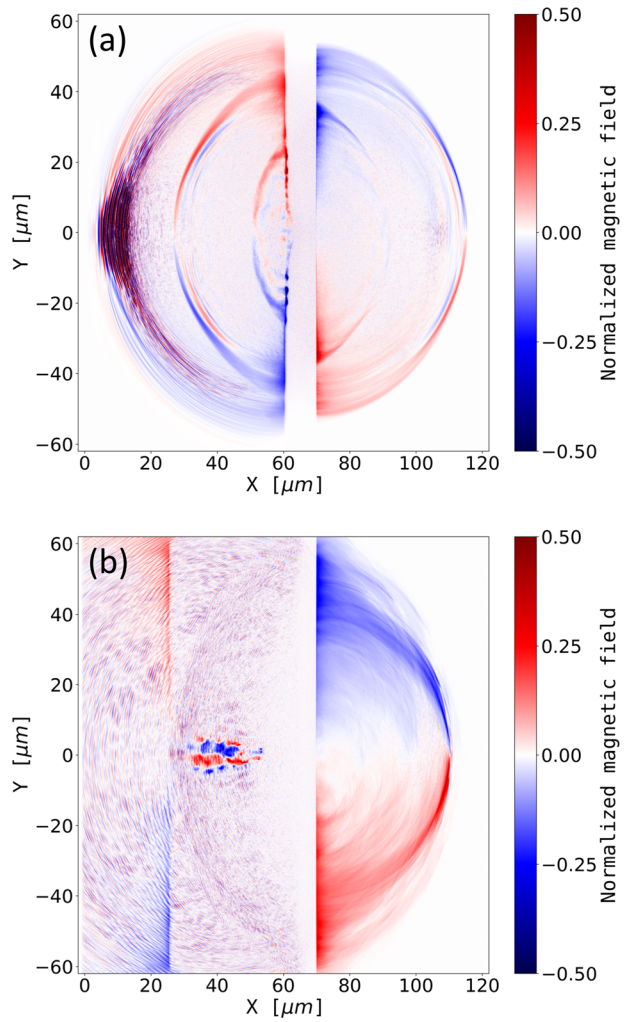

FIG. 6. Snapshots of magnetic fields B_z at $t = 400$ fs (a) without ablation and (b) with 200 ps ablation. The field B_z is in unit of $m_e\omega/|e|$.

The spectra of forward radiation electromagnetic fields in Fig. 6(b) are calculated by fast Fourier transform (FFT) and shown in Fig. 7, which are detected 30 μm away from the laser irradiated spot in the rear surface of the target. Note that this distance is long enough to avoid the interruption of the quasi-static fields produced around the target surface[58] and the noises generated by the target expansion. Here, probe points in the directions larger than 75° are neglected because they are much close to the target surface. Frequency components vary with the detected direction: radiation in large angles is dominant at low frequency (below 10 THz) in the angles between around 5° and 30°, and high frequency components (above 20 THz) become strong and the frequency has a multi-peak structure; this is because in this angular range, there are several secondary weak pulses after the first pulse, which can be seen in Fig. 6(b) as well. The multi-peak profile of field in time domain leads to a multi-peak structure in the frequency spectrum. According to Eq. (2), the corresponding electron energy is around 1∼10 MeV, which is in good agreement with Fig. 4.

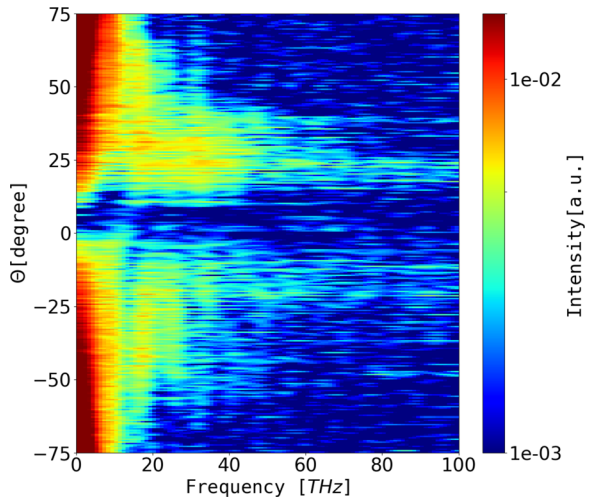

FIG. 7. The spectrum of forward radiation at the right side of the target in the condition with 200 ps ablation.

The energy of THz radiation is calculated by squared amplitude of the Fourier transform of the signal and is then summed up from 0.1 to 30 THz in frequency. The energy angular distribution at the forward direction is illustrated in Fig. 8. It can be seen that for both cases, the radiation is more intense near the target surface because most of the hot electrons have a relatively low energy and their strongest transition radiation is along the target surface. In the condition of 200 ps ablation, the THz radiation is enhanced by approximately one order of magnitude due to both charge and energy increment of electrons. The total energy of THz radiation between $\pm 75^\circ$ is increased by 8.2 times.

IV. CONCLUSION

In conclusion, by introducing a 200 ps mJ ablation pulse before the main laser pulse, an under and near critical ablation preplasma with a scale of tens of micrometers is generated. As a result, the charge and energy of the electrons are substantially improved due to the high energy coupling efficiency between the main laser and the preplasma. Frequency spectra show that the THz radiation is better confined, but it is still distributed in a wide angular range. Moreover, the dominant frequency of the THz radiation is below 10 THz. The angular distribution of THz energy indicates a nearly tenfold enhancement compared to the condition without the target ablation.

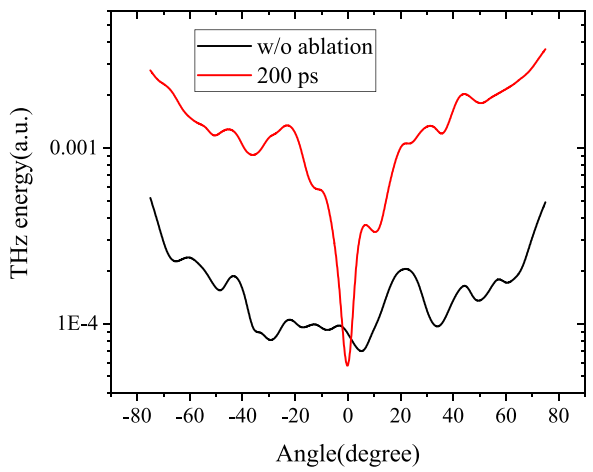

FIG. 8. Angular distributions of energy for THz radiation with ablation (red) and without ablation (black).

ACKNOWLEDGMENTS

This work was supported by the National Basic Research Program of China (Grant No. 2014CB845503), National Natural Science Foundation of China (Grants Nos. 11921006, 11575011, 11975037, 11475010, and 11535001), ITER-CHINA Program (No. 2015GB120001), and National Grand Instrument Project (2012YQ030142). The PIC code EPOCH was in part funded by the UK EPSRC Grant No. EP/G054950/1. Simulations were supported by High-performance Computing Platform of Peking University. The authors thank Doctor Guoqian Liao from Rutherford Appleton Laboratory for his helpful suggestions.

REFERENCES

[1] M. Tonouchi, "Cutting-edge terahertz technology," Nat. Photonics **1**, 97 (2007).
[2] G. P. Williams, "Filling the THz gap–high power sources and applications," Rep. Prog. Phys. **69**, 301 (2006).
[3] T. D. Dorney, R. G. Baraniuk, and D. M. Mittleman, "Material parameter estimation with terahertz time-domain spectroscopy," J. Opt. Soc. Am. A **18**, 1562–1571 (2001).
[4] B. B. Hu and M. C. Nuss, "Imaging with terahertz waves," Opt. Lett. **20**, 1716–1718 (1995).
[5] S. Koenig, D. Lopez-Diaz, J. Antes, F. Boes, R. Henneberger, A. Leuther, A. Tessmann, R. Schmogrow, D. Hillerkuss, R. Palmer *et al.*, "Wireless sub-THz communication system with high data rate," Nat. Photonics **7**, 977 (2013).
[6] C. Kulesa, "Terahertz spectroscopy for astronomy: From comets to cosmology," IEEE Trans. Terahertz Sci. Technol. **1**, 232–240 (2011).
[7] X. Ropagnol, F. Blanchard, T. Ozaki, and M. Reid, "Intense terahertz generation at low frequencies using an interdigitated ZnSe large aperture photoconductive antenna," Appl. Phys. Lett. **103**, 161108 (2013).
[8] D. You, R. Jones, P. Bucksbaum, and D. Dykaar, "Generation of high-power sub-single-cycle 500-fs electromagnetic pulses," Opt. Lett. **18**, 290–292 (1993).
[9] M. Beck, H. Schäfer, G. Klatt, J. Demsar, S. Winnerl, M. Helm, and T. Dekorsy, "Impulsive terahertz radiation with high electric fields from an amplifier-driven large-area photoconductive antenna," Opt. Express **18**, 9251–9257 (2010).
[10] M. Shalaby and C. P. Hauri, "Demonstration of a low-frequency three-dimensional terahertz bullet with extreme brightness," Nat. Commun. **6**, 5976 (2015).
[11] H. Hirori, A. Doi, F. Blanchard, and K. Tanaka, "Single-cycle terahertz pulses with amplitudes exceeding 1 MV/cm generated by optical rectification in linbo 3," Appl. Phys. Lett. **98**, 091106 (2011).
[12] T. Oh, Y. Yoo, Y. You, and K. Kim, "Generation of strong terahertz fields exceeding 8 MV/cm at 1 kHz and real-time beam profiling," Appl. Phys. Lett. **105**, 041103 (2014).
[13] U. Happek, A. Sievers, and E. Blum, "Observation of coherent transition radiation," Phys. Rev. Lett. **67**, 2962 (1991).
[14] G. L. Carr, M. C. Martin, W. R. McKinney, K. Jordan, G. R. Neil, and G. P. Williams, "High-power terahertz radiation from relativistic electrons," Nature **420**, 153 (2002).

[15]Y. Shibata, S. Hasebe, K. Ishi, T. Takahashi, T. Ohsaka, M. Ikezawa, T. Nakazato, M. Oyamada, S. Urasawa, T. Yamakawa *et al.*, "Observation of coherent diffraction radiation from bunched electrons passing through a circular aperture in the millimeter-and submillimeter-wavelength regions," Phys. Rev. E **52**, 6787 (1995).
[16]A. Cook, R. Tikhoplav, S. Y. Tochitsky, G. Travish, O. Williams, and J. Rosenzweig, "Observation of narrow-band terahertz coherent Cherenkov radiation from a cylindrical dielectric-lined waveguide," Phys. Rev. Lett. **103**, 095003 (2009).
[17]Z. Wu, A. S. Fisher, J. Goodfellow, M. Fuchs, D. Daranciang, M. Hogan, H. Loos, and A. Lindenberg, "Intense terahertz pulses from slac electron beams using coherent transition radiation," Rev. Sci. Instrum. **84**, 022701 (2013).
[18]D. Strickland and G. Mourou, "Compression of amplified chirped optical pulses," Opt. Commun. **55**, 447–449 (1985).
[19]G. A. Mourou, C. Barty, and M. D. Perry, "Ultrahigh-intensity laser: Physics of the extreme on a tabletop," Technical Report, Lawrence Livermore National Lab., CA (1997).
[20]S. M. Hooker, "Developments in laser-driven plasma accelerators," Nat. Photonics **7**, 775 (2013).
[21]G. Malka and J. Miquel, "Experimental confirmation of ponderomotive-force electrons produced by an ultrarelativistic laser pulse on a solid target," Phys. Rev. Lett. **77**, 75 (1996).
[22]T. Toncian, C. Wang, E. McCary, A. Meadows, A. Arefiev, J. Blakeney, K. Serratto, D. Kuk, C. Chester, R. Roycroft *et al.*, "Non-Maxwellian electron distributions resulting from direct laser acceleration in near-critical plasmas," Matter Radiat. Extremes **1**, 82 (2016).
[23]Z. Gong, R. Hu, Y. Shou, B. Qiao, C. Chen, F. Xu, X. He, and X. Yan, "Radiation reaction induced spiral attractors in ultra-intense colliding laser beams," Matter Radiat. Extremes **1**, 308 (2016).
[24]W. Leemans, A. Gonsalves, H.-S. Mao, K. Nakamura, C. Benedetti, C. Schroeder, C. Tóth, J. Daniels, D. Mittelberger, S. Bulanov *et al.*, "Multi-GeV electron beams from capillary-discharge-guided subpetawatt laser pulses in the self-trapping regime," Phys. Rev. Lett. **113**, 245002 (2014).
[25]W. Leemans, C. Geddes, J. Faure, C. Tóth, J. Van Tilborg, C. Schroeder, E. Esarey, G. Fubiani, D. Auerbach, B. Marcelis *et al.*, "Observation of terahertz emission from a laser-plasma accelerated electron bunch crossing a plasma-vacuum boundary," Phys. Rev. Lett. **91**, 074802 (2003).
[26]C. Li, M.-L. Zhou, W.-J. Ding, F. Du, F. Liu, Y.-T. Li, W.-M. Wang, Z.-M. Sheng, J.-L. Ma, L.-M. Chen *et al.*, "Effects of laser-plasma interactions on terahertz radiation from solid targets irradiated by ultrashort intense laser pulses," Phys. Rev. E **84**, 036405 (2011).
[27]G. Liao, Y. Li, C. Li, L. Su, Y. Zheng, M. Liu, J. Dunn, J. Nilsen, J. Hunter, W. Wang *et al.*, "Picosecond laser-driven terahertz radiation from large scale preplasmas of solid targets," J. Phys.: Conf. Ser. **717**, 012105 (2016).
[28]G.-Q. Liao, Y.-T. Li, Y.-H. Zhang, H. Liu, X.-L. Ge, S. Yang, W.-Q. Wei, X.-H. Yuan, Y.-Q. Deng, B.-J. Zhu *et al.*, "Demonstration of coherent terahertz transition radiation from relativistic laser-solid interactions," Phys. Rev. Lett. **116**, 205003 (2016).
[29]Y. Li, C. Li, M. Zhou, W. Wang, F. Du, W. Ding, X. Lin, F. Liu, Z. Sheng, X. Peng *et al.*, "Strong terahertz radiation from relativistic laser interaction with solid density plasmas," Appl. Phys. Lett. **100**, 254101 (2012).
[30]G. Liao, Y. Li, C. Li, L. Su, Y. Zheng, M. Liu, W. Wang, Z. Hu, W. Yan, J. Dunn *et al.*, "Bursts of terahertz radiation from large-scale plasmas irradiated by relativistic picosecond laser pulses," Phys. Rev. Lett. **114**, 255001 (2015).
[31]A. Gopal, P. Singh, S. Herzer, A. Reinhard, A. Schmidt, U. Dillner, T. May, H.-G. Meyer, W. Ziegler, and G. Paulus, "Characterization of 700 μJ t rays generated during high-power laser solid interaction," Opt. Lett. **38**, 4705–4707 (2013).
[32]G. Liao, Y. Li, H. Liu, G. G. Scott, D. Neely, Y. Zhang, B. Zhu, Z. Zhang, C. Armstrong, E. Zemaityte *et al.*, "Multimillijoule coherent terahertz bursts from picosecond laser-irradiated metal foils," Proc. Natl. Acad. Sci. **116**, 3994–3999 (2019).
[33]J. Zheng, K. Tanaka, T. Miyakoshi, Y. Kitagawa, R. Kodama, T. Kurahashi, and T. Yamanaka, "Theoretical study of transition radiation from hot electrons generated in the laser–solid interaction," Phys. Plasmas **10**, 2994–3003 (2003).
[34]S. Zhao, C. Lin, H. Wang, H. Lu, X. He, J. Chen, T. Cowan, and X. Yan, "Ion acceleration enhanced by target ablation," Phys. Plasmas **22**, 073106 (2015).
[35]Q. Liao, M. Wu, Z. Gong, Y. Geng, X. Xu, D. Li, Y. Shou, J. Zhu, C. Li, M. Yang *et al.*, "Enhanced laser proton acceleration by target ablation on a femtosecond laser system," Phys. Plasmas **25**, 063109 (2018).
[36]J. Bin, M. Yeung, Z. Gong, H. Wang, C. Kreuzer, M. Zhou, M. Streeter, P. Foster, S. Cousens, B. Dromey *et al.*, "Enhanced laser-driven ion acceleration by superponderomotive electrons generated from near-critical-density plasma," Phys. Rev. Lett. **120**, 074801 (2018).
[37]A. V. Arefiev, B. N. Breizman, M. Schollmeier, and V. N. Khudik, "Parametric amplification of laser-driven electron acceleration in underdense plasma," Phys. Rev. Lett. **108**, 145004 (2012).
[38]D. Wang, Y. Shou, P. Wang, J. Liu, C. Li, Z. Gong, R. Hu, W. Ma, and X. Yan, "Enhanced proton acceleration from an ultrathin target irradiated by laser pulses with plateau ase," Sci. Rep. **8**, 2536 (2018).
[39]A. Pukhov and J. Meyer-ter Vehn, "Relativistic magnetic self-channeling of light in near-critical plasma: Three-dimensional particle-in-cell simulation," Phys. Rev. Lett. **76**, 3975 (1996).
[40]H. Wang, C. Lin, Z. Sheng, B. Liu, S. Zhao, Z. Guo, Y. Lu, X. He, J. Chen, and X. Yan, "Laser shaping of a relativistic intense, short Gaussian pulse by a plasma lens," Phys. Rev. Lett. **107**, 265002 (2011).
[41]K. Estabrook, E. Valeo, and W. Kruer, "Two-dimensional relativistic simulations of resonance absorption," Phys. Fluids **18**, 1151–1159 (1975).
[42]W. Kruer and K. Estabrook, "J × b heating by very intense laser light," Phys. Fluids **28**, 430–432 (1985).
[43]W. Yu, V. Bychenkov, Y. Sentoku, M. Yu, Z. Sheng, and K. Mima, "Electron acceleration by a short relativistic laser pulse at the front of solid targets," Phys. Rev. Lett. **85**, 570 (2000).
[44]Z.-M. Sheng, K. Mima, Y. Sentoku, M. Jovanović, T. Taguchi, J. Zhang, and J. Meyer-ter Vehn, "Stochastic heating and acceleration of electrons in colliding laser fields in plasma," Phys. Rev. Lett. **88**, 055004 (2002).
[45]C. Rousseaux, M. Rabec le Gloahec, S. Baton, F. Amiranoff, J. Fuchs, L. Gremillet, J. Adam, A. Heron, and P. Mora, "Strong absorption, intense forward-Raman scattering and relativistic electrons driven by a short, high intensity laser pulse through moderately underdense plasmas," Phys. Plasmas **9**, 4261–4269 (2002).
[46]Y. Li, J. Zhang, Z. Sheng, J. Zheng, Z. Chen, R. Kodama, T. Matsuoka, M. Tampo, K. Tanaka, T. Tsutsumi *et al.*, "High-energy electrons produced in subpicosecond laser-plasma interactions from subrelativistic laser intensities to relativistic intensities," Phys. Rev. E **69**, 036405 (2004).
[47]A. Pukhov, Z.-M. Sheng, and J. Meyer-ter Vehn, "Particle acceleration in relativistic laser channels," Phys. Plasmas **6**, 2847–2854 (1999).
[48]A. Pukhov, "Strong field interaction of laser radiation," Rep. Prog. Phys. **66**, 47 (2003).
[49]S. P. Mangles, B. Walton, M. Tzoufras, Z. Najmudin, R. Clarke, A. E. Dangor, R. Evans, S. Fritzler, A. Gopal, C. Hernandez-Gomez *et al.*, "Electron acceleration in cavitated channels formed by a petawatt laser in low-density plasma," Phys. Rev. Lett. **94**, 245001 (2005).
[50]B. Liu, H. Wang, J. Liu, L. Fu, Y. Xu, X. Yan, and X. He, "Generating overcritical dense relativistic electron beams via self-matching resonance acceleration," Phys. Rev. Lett. **110**, 045002 (2013).
[51]M. Li, L. Chen, D. Li, K. Huang, Y. Li, Y. Ma, W. Yan, M. Tao, J. Tan, Z. Sheng *et al.*, "Collimated gamma rays from laser wakefield accelerated electrons," Matter Radiat. Extremes **3**, 188 (2018).
[52]A. Arefiev, V. Khudik, A. Robinson, G. Shvets, L. Willingale, and M. Schollmeier, "Beyond the ponderomotive limit: Direct laser acceleration of relativistic electrons in sub-critical plasmas," Phys. Plasmas **23**, 056704 (2016).
[53]G. Garibian, "Contribution to the theory of transition radiation," Sov. Phys. JETP **6**, 1079 (1958).
[54]C. B. Schroeder, E. Esarey, J. van Tilborg, and W. P. Leemans, "Theory of coherent transition radiation generated at a plasma-vacuum interface," Phys. Rev. E **69**, 016501 (2004).
[55]R. Ramis, R. Schmalz, and J. Meyer-ter Vehn, "Multi—A computer code for one-dimensional multigroup radiation hydrodynamics," Comput. Phys. Commun. **49**, 475–505 (1988).

[56]P. Gibbon, *Short Pulse Laser Interactions with Matter* (World Scientific Publishing Company, Singapore, 2004).
[57]T. Arber, K. Bennett, C. Brady, A. Lawrence-Douglas, M. Ramsay, N. Sircombe, P. Gillies, R. Evans, H. Schmitz, A. Bell *et al.*, "Contemporary particle-in-cell approach to laser-plasma modelling," Plasma Phys. Controlled Fusion **57**, 113001 (2015).
[58]W. Ding and Z. Sheng, "Sub gv/cm terahertz radiation from relativistic laser-solid interactions via coherent transition radiation," Phys. Rev. E **93**, 063204 (2016).
[59]W. Ding, Z. Sheng, and W. Koh, "High-field half-cycle terahertz radiation from relativistic laser interaction with thin solid targets," Appl. Phys. Lett. **103**, 204107 (2013).